Bull. Mater. Sci., Vol. 36, No. 3, June 2013, pp. 429–435. © Indian Academy of Sciences.

Effect of bias voltage on microstructure and mechanical properties of arc evaporated (Ti, Al)N hard coatings

F ALIAJ[1,*], N SYLA[1], S AVDIAJ[1] and T DILO[2]

[1]Department of Physics, Faculty of Mathematical and Natural Sciences, University of Prishtina, Rr. Nëna Terezë nr. 5, 10000 Prishtina, Kosovo

[2]Department of Physics, Faculty of Natural Sciences, University of Tirana, Bulevardi Zogu i Parë, Tirana, Albania

MS received 17 April 2012

Abstract. **In the present study, authors report on the effect that substrate bias voltage has on the microstructure and mechanical properties of (Ti, Al)N hard coatings deposited with cathodic arc evaporation (CAE) technique. The coatings were deposited from a $Ti_{0.5}Al_{0.5}$ powder metallurgical target in a reactive nitrogen atmosphere at three different bias voltages: $U_B = -25$, -50 and -100 V. The coatings were characterized in terms of compositional, microstructural and mechanical properties. Microstructure of the coatings was investigated with the aid of X-ray diffraction in glancing angle mode, which revealed information on phase composition, crystallite size, stress-free lattice parameter and residual stress. Mechanical properties were deduced from nano-indentation measurements. The residual stress in all the coatings was compressive and increased with increasing bias voltage in a manner similar to that reported in literature for Ti–Al–N coatings deposited with CAE. The bias voltage was also found to significantly influence the phase composition and crystallite size. At -25 V bias voltage the coating was found in single phase *fcc*-(Ti, Al)N and with relatively large crystallites of ∼9 nm. At higher bias voltages (-50 and -100 V), the coatings were found in dual phase *fcc*-(Ti, Al)N and *fcc*-AlN and the size of crystallites reduced to approximately 5 nm. The reduction of crystallite size and the increase of compressive residual stress with increasing bias voltage both contributed to an increase in hardness of the coatings.**

Keywords. **Hard coatings; cathodic arc evaporation; GAXRD; hardness; (Ti, Al)N.**

1. Introduction

The cathodic arc evaporation (CAE) method is a versatile, efficient and high productivity physical vapour deposition (PVD) technique used for deposition of Ti–Al–N hard coatings (Coll *et al* 1992; Vlasveld *et al* 2002; Ahlgren and Blomqvist 2005), as it produces dense and adherent coatings and at high deposition rates, having a wide range of applications in various fields. Ti–Al–N CAE-produced hard coatings significantly increase lifetime and performance of cutting tools and machine parts that are subjected to extremely difficult conditions (Freller and Haessler 1988; Coll *et al* 1992; Prengel *et al* 2001; PalDey and Deevi 2003). A big advantage of CAE is a relatively high level of ionizing atoms in the plasma, which makes it possible to control the energy of the ions arriving at the substrate by the application of bias voltage.

Negative substrate bias voltage is a well-described tool and an important process parameter to tailor the morphology, microstructure and mechanical properties of Ti–Al–N coatings. The bias voltage during the coating process is a highly influential parameter as it controls energy of the ions arriving at the substrate. At low bias voltage levels (0 to -100 V), the residual stress increases with increasing bias voltage due to an increase of defect density, which is also connected with an increase in hardness. At higher bias voltages, the ion bombardment induced mobility of atoms, which promotes the annihilation of defects, reduces the residual stress and consequently the hardness also drops (Ljungcrantz *et al* 1995; Odén *et al* 1999; Vlasveld *et al* 2002; Sato *et al* 2003; Ahlgren and Blomqvist 2005; Pfeiler *et al* 2007, 2008).

In recent publications, Pfeiler *et al* (2007, 2008) found the bias voltage to be an important parameter to influence the phase composition of Ti–Al–V–N and Ti–Al–Ta–N coatings. The phase composition and thus the microstructure and properties of (Ti, Al)N coatings are usually tailored by varying the Al contents. However, the maximum solubility limit of Al in *fcc*-(Ti, Al)N depends strongly on the PVD technique that used to grow the films and is influenced primarily by the deposition parameters (PalDey and Deevi 2003; Bujak *et al* 2004). Recently, it was shown that the maximum solubility limit of Al in *fcc*-(Ti, Al)N can be varied from 0·64 to 0·74 by affecting the Al distribution on the metal sublattice (Mayrhofer *et al* 2006). Therefore, the mechanism that influences the Al distribution during film growth can influence the phase stability of supersaturated *fcc*-(Ti, Al)N.

In this study, the (Ti, Al)N coatings were deposited with CAE technique at three different bias voltages, while other

*Author for correspondence (fisnik.aliaj@uni-pr.edu)

deposition parameters were kept constant. Glancing angle X-ray diffraction and glow discharge optical emission spectroscopy were used to characterize the structure and chemical composition of the coatings. Indentation hardness and Young's modulus were also studied. The authors illustrate the interplay between bias voltage, several microstructure parameters and hardness and in particular, the information contents of the partial coherence of crystallites. Based on the found results, the authors suggest a microstructure formation model for (Ti, Al)N coatings deposited with CAE.

2. Experimental

2.1 *Deposition of coatings*

The coatings investigated in this work were deposited by cathodic arc evaporation (CAE) using a hard coating unit $\pi 300$ from PLATIT. The cathode used to deposit the coatings was a PLANSEE $Ti_{0·5}Al_{0·5}$ target produced by powder metallurgy. The depositions were done at three different substrate bias voltages (U_B): −25, −50 and −100 V (producing in this way three coatings in total), in order to modify the energy of ions arriving at the substrate. The depositions were performed under N_2 atmosphere maintained at a working pressure of 5 Pa. The deposition temperature was ∼500 °C, the deposition time was 160 min for all the runs, the current on the target was 300 A and the magnetic field of 2·5 T was used for confinement of the arc discharge. Mirror-polished plates of cemented carbides (WC–Co) were used as substrates as usual for coatings considered for high temperature applications.

The coatings were characterized in terms of chemical composition, microstructure, mechanical properties and coating thickness.

2.2 *Chemical composition analysis*

The chemical composition of coatings was estimated by the glow discharge optical emission spectroscopy (GDOES) using a commercial surface depth profile instrument GDS-750A from Leco. The sputtering area of 4 mm in diameter, was studied in a constant power mode and at an Ar flow of 400 sccm.

2.3 *Microstructure analysis*

X-ray diffraction in glancing-angle mode (GAXRD) was employed to evaluate the phase composition, cluster size, crystallite size and their mutual disorientation, stress-free lattice parameter and residual stress. GAXRD experiments were performed on a Bruker D8 Advance diffractometer that was equipped with a CuKα (λ = 0·15418 nm) target, with a parabolic Göebel mirror in the primary beam and a Soller collimator with the acceptance angle of 0·12° and a flat LiF monochromator that were situated in the diffracted beam in front of the scintillation detector. LiF monochromator nearly suppressed the CuKα2 spectral line (Kα2/Kα1 = 0·08). The diffraction patterns were taken at an angle of incidence $\gamma = 3°$ by scanning between 2θ values of 20 and 159° with a step size of 0·05°.

2.4 *Mechanical properties*

The indentation hardness, H_{IT}, of the coatings was measured using the nano-indentation tester from CSM instruments equipped with a Berkovich indenter and considering the Oliver and Pharr (1992) method. The relative humidity in the room was ∼50% and the temperature was ∼25 °C for all the measurements. Due to high surface roughness, the coatings were first locally polished with a diamond suspension paste of 0·5–1·0 μm. The coatings were then ultrasonically cleaned in acetone. Prior to the measurements, a tip calibration procedure was performed on a fused silica standard (ν = 0·17). There were 20 indents made per coating. The loading and unloading rates were 80 mN/min and at a maximum load of 40 mN, for all the measurements. This resulted in the maximum penetration depth of ∼0·2 μm, which is below 10% of coating thickness—a requirement in order to avoid the influence from the substrate.

2.5 *Coating thickness*

Coating thickness was measured with ball-crater experiments using a Compact Calotest Instrument from CSM. The ball diameter was 30 mm and the slurry particle size was 2–10 μm, for all the measurements. For calculation of the thickness, for each coating, three depressions in random positions were made and the presented results are mean values. It is worth to mention that a rough estimation of coating thickness can also be made from GDOES depth-compositional profiles.

3. Results and discussion

3.1 *Chemical composition*

The results of a typical compositional analysis carried out by GDOES is shown in figure 1. The vertical dotted lines denote the range that was taken for the calculation of the averaged atomic percent (at%) of the elements present in the samples. The reason for taking such a narrow range was to be far enough from the surface as it is clearly contaminated with oxygen and from the influence of the substrate elements, especially carbon, as we wanted to calculate the atomic percent of the coating elements as precisely as possible. Results deduced from GDOES analysis show that the [Al]/([Al]+[Ti]) atomic ratio in the coatings is higher than that in the evaporation target, and that there is a slight increase of [Al]/([Al]+[Ti]) atomic ratio as the bias voltage is increased (figure 2).

Since coatings thicknesses are the same (see table 1), within the experimental accuracy of the method and

deposition time was the same for all runs, we conclude that there was no influence of the negative bias voltage on the growth rate of the deposited samples. Romero *et al* (2006) have observed, for Cr–Al–N coatings deposited by CAE method, a decrease in growth rate with increasing bias voltage, and they have attributed this behaviour to a partial re-sputtering mechanism induced by ion bombardment during film growth. This mechanism was also responsible for a slight increase of Cr/Al composition as the negative bias increased. Similar results were obtained by others (Freller and Haessler 1988; Coll *et al* 1992; Vlasveld *et al* 2002; Ahlgren and Blomqvist 2005)

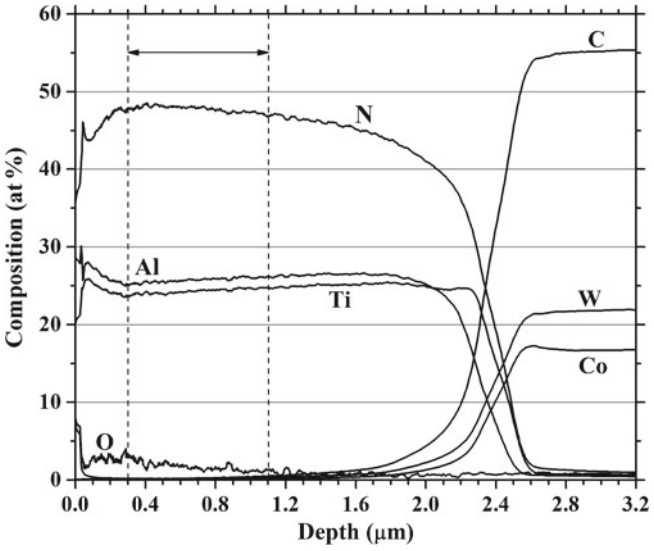

Figure 1. GDOES compositional profile of coating deposited at $U_B = -25$ V. Vertical dotted lines denote range that was used for calculation of at% of elements present in coating.

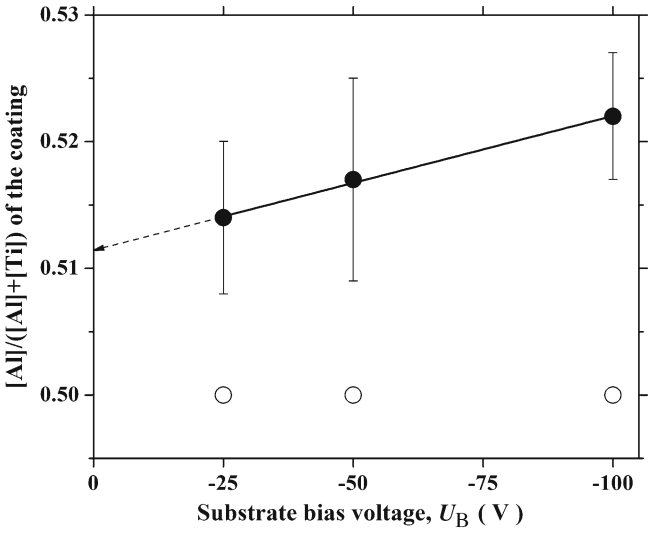

Figure 2. [Al]/([Al]+[Ti]) atomic ratio of coatings as a function of bias voltage. Open circles denote [Al]/([Al]+[Ti]) atomic ratios of target used to deposit coatings. Solid line is a linear fit to data points.

Table 1. Some physical properties, microstructure features and GDOES results of (Ti, Al)N coatings deposited at different bias voltages.

U_B (V)	Thickness, t (μm)	Hardness, H_{IT} (GPa)	Young's modulus, E (GPa)	Residual stress, σ (GPa)	Stress-free lattice parameter, a_0 (nm)	Crystallite size, D (nm)	Mutual disorientation, ω (°)	N (at%)	O (at%)
−25	2·6 ± 0·1	20·7 ± 1·1	589 ± 21	−1·75 ± 0·29	0·4158 ± 0·0002	8·5 ± 0·3	0·32 ± 0·05	47·8 ± 0·4	1·7 ± 0·5
−50	2·8 ± 0·1	22·6 ± 1·2	585 ± 23	−5·94 ± 0·27	0·4176 ± 0·0002	5·8 ± 0·1	0·56 ± 0·07	50·1 ± 0·5	1·2 ± 0·5
−100	2·7 ± 0·1	23·1 ± 1·2	561 ± 23	−7·51 ± 0·46	0·4177 ± 0·0003	4·7 ± 0·2	0·69 ± 0·09	49·9 ± 0·6	1·1 ± 0·3

for Ti–Al–N coatings deposited by arc evaporation method. Therefore, in the light of Romero *et al* (2006) work and others, we can conclude that there was no sputtering mechanism induced by ion bombardment that would be responsible for the observed differences of coating composition compared to target composition. The mechanism behind the Al enrichment is attributed to the lower melting point of Al than Ti and to the relatively large arc current used to deposit the coatings. The high arc current may give rise to arc by spot splitting, which in turn may result in an increased evaporation rate of Al more than Ti.

3.2 *Phase composition, stress-free lattice parameter and residual stress*

Crystallographic structure of the coatings investigated in this work, as obtained from GAXRD, are shown in figure 3. Vertical dotted lines indicate the expected peak positions for the respective phases. For the phases: *fcc*-TiN, *fcc*-AlN, w-AlN and WC values for peak positions were taken from PDF-2 (ICDD 1997). For *fcc*-(Ti, Al)N phase, the expected peak positions were calculated using Braggs' law and a value for lattice parameter $a = 0{\cdot}419$ nm (Inamura *et al* 1987). All the *fcc*-(Ti, Al)N peaks of the coatings under study are shifted to higher/lower diffraction angles than the standard value of *fcc*-TiN/*fcc*-AlN. This is due to the incorporation of the smaller Al atoms into the *fcc*-TiN lattice. Thus, GAXRD results confirm limited solubility of Al in the host structure of TiN. In all the coatings, the dominating phase is *fcc*-(Ti, Al)N

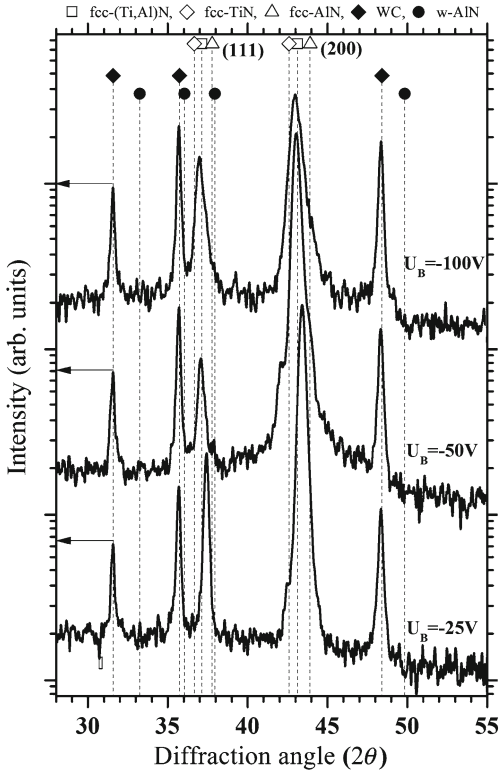

Figure 3. Part of GAXRD patterns of (Ti, Al)N coatings investigated in this work.

(NaCl structure, space group $Fm{-}3m$), although there were traces of *fcc*-AlN (NaCl structure, space group $Fm{-}3m$), and possibly w-AlN (wurtzite-type structure, space group $P63mc$) detected by XRD for the coatings deposited at bias voltages −50 and −100 V. The diffraction lines corresponding to *fcc*-(Ti, Al)N phase overlap with diffraction lines from *fcc*-AlN phase which possesses smaller lattice parameter. The lattice parameter of the detected *fcc*-AlN peaks was calculated to be between 0·4108 and 0·4124 nm, which are in good agreement with PDF-2 (ICDD 1997). With increasing bias voltage, the *fcc*-(Ti, Al)N peaks get shifted to lower diffracting angles and get broader. This indicates an increase of residual stress state in the coatings and a reduction of crystallite size with increasing bias voltage, a matter to be discussed briefly.

The arrowed horizontal solid lines in figure 3 show a selected substrate peak and its development with bias voltage. Increasing bias voltage increases height of the peak, and since the thickness of the coatings is the same, within the experimental accuracy of the method, then the only explanation for this behaviour is the increase of aluminum content with increasing bias voltage. The increase of aluminum content decreases the linear absorption coefficient and consequently the penetration depth for X-ray increases, giving more information from the substrate, i.e. higher substrate peaks. The same is true for all substrate peaks of the samples under study. Therefore, results obtained from GAXRD confirm results obtained from GDOES, i.e. the aluminum content increases with increasing bias voltage.

In GAXRD patterns of all coatings, only peaks from *fcc*-(Ti, Al)N, substrate (WC) and some weaker *fcc*-AlN were visible. All the GAXRD patterns were fitted with Pearson-VII function by means of a peak-by-peak least-square refinement. This procedure was useful in determining several peak parameters, including exact position (2θ) and integral breadth (β), which were used in further analysis. The individual lattice parameters of the *fcc*-(Ti, Al)N phase were calculated from peak positions. In cubic materials under uniaxial stress, the individual lattice parameters, a_ψ, depend linearly on $\sin^2\psi$ (Rafaja *et al* 2006a, 2011):

$$a_\psi = a_\perp + (a_\parallel - a_\perp)\sin^2\psi, \tag{1}$$

where $a_\perp$ and $a_\parallel$ are the lattice parameters perpendicular and parallel to sample surface, which are directly obtained from $\sin^2\psi$-plot at $\sin^2\psi = 0$ and $\sin^2\psi = 1$, respectively; $\psi = \theta - \gamma$ is the angle between the diffracting lattice planes and the sample surface. Then, the stress-free lattice parameter and residual stress were calculated according to equations (Rafaja *et al* 2006a, 2011):

$$a_0 = a_\perp + \frac{2\nu}{1+\nu}\left(a_\parallel - a_\perp\right) \tag{2}$$

and

$$\sigma = \frac{a_0 - a_\perp}{a_0}\frac{E}{2\nu}. \tag{3}$$

For calculation of the preceding parameters, Young's modulus, E, obtained from nano-indentation measurements and Poisson ratio, $\nu = 0{\cdot}3$ were used.

The comparison of the stress-free lattice parameter, as calculated from (2), with the anticipated Vegard-like dependence of the intrinsic lattice parameter on the overall titanium content in the coatings is shown in figure 4. The Vegard-like dependence is shown by the solid line and the equation for this line is taken from Rafaja *et al* (2008). The stress-free lattice parameter of the coating deposited at −25 V bias voltage (filled rectangle in figure 4) is lesser than the lattice parameter anticipated from Vegard-like dependence. The nitrogen content in this coating, as measured by GDEOS, is lesser than the expected value of 50 at% (see table 1). This indicates that some nitrogen must be missing in the *fcc*-(Ti, Al)N phase present in the sample, making the lattice structure to deform and shrink, and as a consequence the stress-free lattice parameter in this phase is lower than the value expected from Vegard-like dependence. The stress-free lattice parameter of the coatings deposited at −50 and −100 V bias voltages (half-filled symbols) is higher than the value anticipated from Vegard-like dependence. The Al content as measured from GDOES is ∼52 at%, whereas the lattice parameter has a value that corresponds to Al content of ∼46 at% in *fcc* phase, i.e. $Ti_{(0{\cdot}54\pm0{\cdot}2)}Al_{(0{\cdot}46\pm0{\cdot}02)}N$. Therefore, the phase *fcc*-(Ti, Al)N has less Al (about 6 at%) than it corresponds to overall Al content as measured by GDOES. A possible explanation is that Al, which is missing in *fcc*-(Ti, Al)N, forms another phase (Rafaja *et al* 2011). Assuming that the other phase is *fcc*-AlN, then the phase composition of the coatings, deposited at −50 and −100 V bias voltage, can be estimated to be (93 ± 3) mol% *fcc*-$Ti_{(0{\cdot}54\pm0{\cdot}2)}Al_{(0{\cdot}46\pm0{\cdot}02)}N$ and (7 ± 3) mol% *fcc*-AlN. The co-existence of two *fcc* phases with different stress-free lattice parameters indicate fluctuations in the Ti and Al concentrations, that are typical of spinoidal decomposition in this system (Wüstefeld *et al* 2010 and references therein).

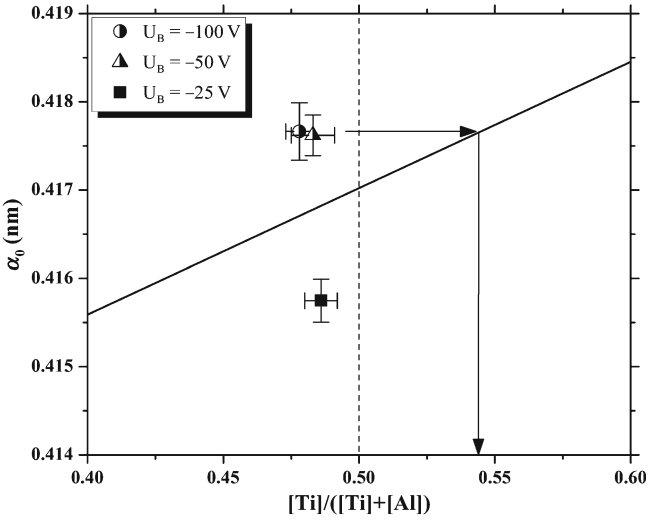

Figure 4. Comparison of stress-free lattice parameter with Vegard-like dependence. Vegard-like dependence is shown by solid line and equation for this line is taken from Rafaja *et al* (2008). Vertical dotted line represents titanium content of target used to deposit coatings. Filled rectangle represents coating with only *fcc*-(Ti, Al)N phase present. Half-filled symbols represent coatings with mixture of *fcc*-(Ti, Al)N and *fcc*-AlN phase.

The results of residual stress in *fcc*-(Ti, Al)N phase, calculated using the approach described above, are presented in table 1. The residual stress in the *fcc*-(Ti, Al)N phase of all the coatings was compressive. Negative bias voltage has been found to strongly influence the stress state in the coatings. An increase of negative bias voltage from −25 to −50 V resulted in an increase of compressive residual stress for about 4 GPa, while further increasing the negative bias voltage to −100 V resulted only in a slight increase of compressive residual stress. An increase of compressive residual stress with increasing bias voltage is a well-reported phenomenon (Ljungcrantz *et al* 1995; Vlasveld *et al* 2002; Sato *et al* 2003; Wüstefeld *et al* 2010). The largest values of residual stress are found in the coatings where the second *fcc*-AlN phase is introduced. Similar results were obtained by Wüstefeld *et al* (2010).

3.3 *Hardness*

The hardness of the (Ti, Al)N coatings increased with increasing negative bias voltage, as presented in table 1. The largest increase of hardness was observed when bias voltage increased from −25 to −50 V. Further increasing the bias voltage resulted only in a slight increase of hardness. The coating deposited at −25 V bias voltage containing single phase *fcc*-(Ti, Al)N structure with relatively large crystallites and low compressive residual stress exhibit lower hardness. The coatings deposited at higher bias voltages (−50 and −100 V) containing dual-phase *fcc*-(Ti, Al)N and *fcc*-AlN structure with smaller crystallites and larger residual stress showed much higher values of hardness. Thus, it seems that the increase in hardness is associated with the introduction of the second *fcc*-AlN phase in the coatings. The hardness seems to follow similar relationship as residual stress with bias voltage. Furthermore, the hardness was found to increase with the decreasing crystallite size following Hall–Petch like dependence. This relationship between crystallite size and hardness and the contribution of the residual stress to the hardness of the Ti–Al–N and Ti–Al–X–N (X = Si and V) hard coatings deposited by CAE technique is frequently reported in literature (Rafaja *et al* 2006b, 2007; Pfeiler *et al* 2007; Wüstefeld *et al* 2010).

3.4 *Cluster size, crystallite size and their mutual disorientation*

A detailed XRD line profile analysis showed that the coatings under study consist of partially coherent crystallites with very small mutual disorientation (figure 5). This phenomenon of crystallographic coherence was described

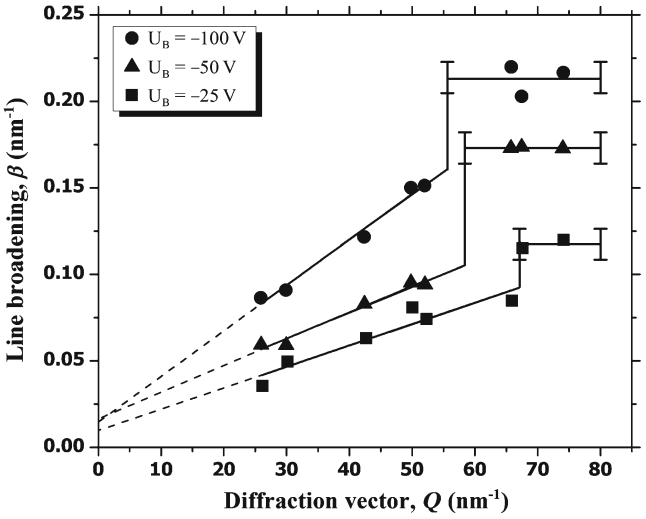

Figure 5. Dependence of XRD line broadening on size of diffraction vector (for further details, see text).

theoretically by Rafaja *et al* (2004) by a partial overlap of the broadened reciprocal lattice points for crystallites smaller than ∼10 nm that causes a 'narrowing' of XRD lines in nanocrystalline materials, and is illustrated in many examples (Rafaja *et al* 2004, 2006a,b, 2007, 2008, 2011; Wüstefeld *et al* 2010). In general, such highly preferentially oriented crystallites are a result of the local epitaxy or of the fragmentation of larger crystallites (Wüstefeld *et al* 2010). From the dependence of XRD line broadening on the size of the diffraction vector, three microstructure parameters were calculated: the average size of clusters which consisted of partially coherent *fcc*-(Ti, Al)N crystallites, average size of the crystallites and their mutual disorientation. The size of crystallites was calculated from the maximum line broadening (constant part of the line broadening in figure 5). The reciprocal of the maximum line broadening corresponds to the size of the crystallites. The mutual disorientation was calculated from the diffraction vector for which the line broadening steeply increases and the size of the crystallites. The size of the clusters was calculated from the extrapolation of the line broadening to the zero diffraction vector (dotted lines in figure 5). The average size of the clusters is inversely proportional to the intercept of the extrapolated line broadening. However, since the extrapolated line broadening for coatings in this study are very close to zero and since the error in estimating the cluster size strongly depends on the error in determining the intercept, it could only be concluded that the average cluster size is between 40 and 120 nm. Furthermore, we see that the extrapolated line broadening and thus the cluster size does not depend, within the experimental accuracy of the XRD method, on the negative bias voltage. The sizes of partially coherent crystallites and their mutual disorientation are given in table 1.

Based on the results presented above, the following can be suggested on the microstructure formation of the (Ti, Al)N hard coatings deposited by CAE. In CAE, the coatings are deposited in clusters with the size between 40 and 120 nm. The size of the clusters does not change, within experimental accuracy of the method of the XRD line profile analysis, with negative bias voltage. The coating deposited at −25 V bias voltage contained single phase *fcc*-(Ti, Al)N, the deposition was done in clusters that were composed of partially coherent crystallites with a size of ∼9 nm with very small mutual disorientation; the coating was under a relatively low-compressive residual stress of ∼2 GPa and the hardness was ∼21 GPa. Increasing negative bias voltage to −50 V leads to formation of dual-phase coating (90–96 mol% *fcc*-(Ti, Al)N and 4–10 mol% *fcc*-AlN), to an increase of compressive residual stress to about 6 GPa, to a substantial reduction of crystallite size and the increase of their mutual disorientation. Both the increase of compressive residual stress and the reduction of crystallite size contribute to the increase of the hardness ∼10%. Further increasing bias voltage to −100 V did not contribute to substantial changes in microstructure and mechanical properties as compared to when bias voltage increased from −25 to −50 V, as can be seen in table 1.

The bias voltage is a very influential deposition parameter as it controls the energy of the bombarding ions that arrive at the substrate. Increasing bias voltage increases the energy of the bombarding ions. The ion bombardment causes two concurrent effects. First, it increases the defect density. Second, it also increases adatom mobility and diffusivity and thus the ability of annihilation of defects (Pfeiler *et al* 2007). These ion bombardment induced defects lead to an apparent fragmentation of clusters into partial coherent crystallites with very small mutual disorientation and to the development of local fluctuations in Ti and Al within (Ti, Al)N that lead, at higher bias voltages, to the formation of *fcc*-AlN as a second phase (Wüstefeld *et al* 2010). From −25 to −50 V bias voltages, the process of generating defects seems to be the predominant one. In this bias range, we observed the largest changes in mechanical and microstructure parameters. From −50 to −100 V bias voltages, the induced mobility of adatoms may have led to the annihilation of some defects, which is observed as not so a large change in mechanical and microstructural parameters.

4. Conclusions

In this study, the effects that bias voltage has on the mechanical properties and microstructure formation in the cathodic-arc evaporation-deposited (Ti, Al)N coatings was investigated. The study was done by means of XRD in glancing-angle geometry, GDOES and nano-indentation measurements.

It was shown that the Al content of the coatings was slightly higher than that of the target used to deposit the coatings, and this was attributed to the lower melting point of Al than Ti and to the relatively large arc current used to deposit the coatings. The coatings were deposited in clusters with size between 40 and 120 nm. The size of the

clusters did not change with bias voltage. The bias voltage was shown to lead to an apparent fragmentation of clusters into partially coherent crystallites with very small mutual disorientation. While the negative bias voltage has no effect on the cluster size, size of the crystallites decreases and their mutual disorientation increases with increasing bias voltage. The bias voltage was also shown to influence the phase composition and the residual stress of the coatings. At −25 V bias voltage, the coating was found in single phase *fcc*-(Ti, Al)N and with relatively small compressive residual stress. At higher bias voltages (−50 and −100 V), the coatings were found in dual phase *fcc*-(Ti, Al)N and *fcc*-AlN and with relatively large compressive residual stress. The reduction of crystallite size and increase of compressive residual stress with increasing bias voltage both contributed to an increase in hardness of the coatings.

Acknowledgements

The authors greatly appreciate the German Academic Exchange Service (DAAD) for the financial support obtained for the educational journey to TU-BA Freiberg, Germany, where the investigation was performed.

References

Ahlgren M and Blomqvist H 2005 *Surf. Coat. Technol.* **200** 157

Bujak J, Walkowicz J and Kusiñski J 2004 *Surf. Coat. Technol.* **180–181** 150

Coll B F, Sathrum P, Fontana R, Peyre J P, Duchateau D and Benmalek M 1992 *Surf. Coat. Technol.* **52** 57

Freller H and Haessler H 1988 *Surf. Coat. Technol.* **36** 219

ICDD, International Center for Diffraction Data, PDF-2 on CD-ROM, Philadelphia, PA, 1997

Inamura S, Nobugai K and Kanamaru K 1987 *J. Solid State Chem.* **68** 124

Ljungcrantz H, Hultman L, Sundgren J E and Karlsson L 1995 *J. Appl. Phys.* **78** 832

Mayrhofer P H, Musil D and Schneider J M 2006 *J. Appl. Phys.* **100** 094906

Odén M, Almer J and Håkansson G 1999 *Surf. Coat. Technol.* **120–121** 272

Oliver W C and Pharr G M 1992 *J. Mater. Res.* **7** 1564

PalDey S and Deevi S C 2003 *Mater. Sci. Eng.* **A342** 58

Pfeiler M, Kutschej K, Penoy M, Michotte C, Mitterer C and Kathrein M 2007 *Surf. Coat. Technol.* **202** 1050

Pfeiler M, Fontalvo G A, Wagner J, Kutschej K, Penoy M, Michotte C, Mitterer C and Kathrein M 2008 *Tribol. Lett.* **30** 91

Prengel H G, Jindal P C, Wendt K H, Santhanam A T, Hegde P L and Penich R M 2001 *Surf. Coat. Technol.* **139** 25

Rafaja D, Klemm V, Schreiber G, Knapp M and Kužel R 2004 *J. Appl. Crystallogr.* **37** 613

Rafaja D, Dopita M, Růžička M, Klemm V, Heger D, Schreiber G and Šíma M 2006a *Surf. Coat. Technol.* **201** 2835

Rafaja D, Poklad A, Klemm V, Schreiber G, Heger D, Šíma M and Dopita M 2006b *Thin Solid Films* **514** 240

Rafaja D, Poklad A, Klemm V, Schreiber G, Heger D and Šíma M 2007 *Mater. Sci. Eng.* **A462** 279

Rafaja D, Wüstefeld C, Dopita M, Klemm V, Heger D, Schreiber G and Šíma M 2008 *Surf. Coat. Technol.* **203** 572

Rafaja D, Wüstefeld C, Baehtz C, Klemm V, Dopita M, Motylenko M, Michotte C and Kathrein M 2011 *Metal. Mater. Trans. A* **42** 559

Romero J, Gómez M A, Esteve J, Montalà F, Carreras L, Grifol M and Lousa A 2006 *Thin Solid Films* **515** 113

Sato K, Ichimiya N, Kondo A and Tanaka Y 2003 *Surf. Coat. Technol.* **163–164** 135

Vlasveld A C, Harris S G, Doyle E D, Lewis D B and Munz W D 2002 *Surf. Coat. Technol.* **149** 217

Wüstefeld Ch, Rafaja D, Klemm V, Michotte C and Kathrein M 2010 *Surf. Coat. Technol.* **205** 1345